Available online at www.sciencedirect.com

jmr&t Journal of Materials Research and Technology

journal homepage: www.elsevier.com/locate/jmrt

Original Article

Optical response, lithiation and charge transfer in Sn-based 211 MAX phases with electron localization function

M.A. Hadi [a,*], N. Kelaidis [b,c], P.P. Filippatos [b,d], S.-R.G. Christopoulos [d], A. Chroneos [e,f], S.H. Naqib [a], A.K.M.A. Islam [a,g]

[a] Department of Physics, University of Rajshahi, Rajshahi, 6205, Bangladesh
[b] Institute of Nanoscience and Nanotechnology (INN), National Center for Scientific Research 'Demokritos', 15310, Agia Paraskevi, Athens, Greece
[c] Theoretical and Physical Chemistry Institute, National Hellenic Research Foundation, Vass. Constantinou 48, GR-11635 Athens, Greece
[d] Faculty of Engineering, Environment and Computing, Coventry University, Priory Street, Coventry CV1 5FB, United Kingdom
[e] Department of Electrical and Computer Engineering, University of Thessaly, 38221, Volos, Greece
[f] Department of Materials, Imperial College, London, SW7 2AZ, UK
[g] International Islamic University Chittagong, Kumira, Chittagong, 4318, Bangladesh

ARTICLE INFO

Article history:
Received 19 January 2022
Accepted 12 March 2022
Available online 29 March 2022

Keywords:
MAX phases
Optical response
Lithiation
Charge transfer
Electron localization function

ABSTRACT

In this study, optical response, lithiation and charge transfer in existing M_2SnC MAX phases with electron localization function (ELF) were investigated for the first time using the density functional theory (DFT). Calculations show that the non-zero value of $\varepsilon_1(0)$ is an indication of the large availability of free charge carriers in these metallic systems. High reflection of light at the low frequencies indicates the high conductivity and low absorption power of the studied materials. In the visible light region, the average reflectivity of M_2SnC is more than 40%, making them potential coating materials for reducing solar heating with greater possibility for Nb_2SnC. M_2SnC phases are optically anisotropic. The static absorption coefficient represents the universal non-zero value for the hexagonal M_2SnC phases. The Plasma frequency is found to be slightly larger for ⟨001⟩ polarization. Lithium (Li) incorporation into M_2SnC show that the formation energy required for Li incorporation into Lu_2SnC is low, and therefore, it should be suitable for use as an anode in battery. The chemical bonds (M–X) between transition metal ions and carbon are expected to be strong localized bonds as predicted from the ELF maps. The bonds (M–Sn) between transition metal M and A-group element Sn are less localized and more spread out, possibly pointing to a weaker bond. The magnitude of the Bader charges is significantly larger compared to the Mulliken and Hirshfeld charges. According to Bader analysis,

* Corresponding author.
E-mail address: hadipab@gmail.com (M.A. Hadi).
https://doi.org/10.1016/j.jmrt.2022.03.083

maximum charge transfer occurs in Hf_2SnC and minimum charge transfer occurs in V_2SnC.

1. Introduction

A new class of ternary layered transition metal carbides, nitrides and borides, known as MAX phases, crystallizes with a chemical formula $M_{n+1}AX_n$, where n is the layer index that varies from 1 to 6, M is a transition metal, A is an A-group element and X is either C or N or B [1,2]. Depending on the layer index n, MAX phases are marked as 211, 312, 413, 514, 615, and 716 phases for $n = 1, 2, 3, 4, 5,$ and 6, respectively [2]. In the 211 phases ($n = 1$), two M layers appear between the two A layers, while in the 312 phases ($n = 2$), three M layers occupy the space between the two A layers. Similarly, in the 413 phases ($n = 3$) four M layers exist between the two A layers. The same pattern can be seen in the other 514, 615, and 716 phases. M forms the ceramic layer with X where the A-layer is purely metallic. Due to their layered structure, the MAX phases exhibit a unique combination of mechanical, electrical and thermal properties, some of which are common properties of metals and some of which are inherent in ceramics [3]. The common metallic properties are thermal and electrical conductivities, machinability, high fracture toughness, damage tolerance and thermal shock resistance. The innate ceramic properties are low density, high elastic stiffness, oxidation and corrosion resistance, resistant to fatigue and creep and ability to maintain the mechanical strength up to high temperature [4]. Due to the combination of the above mentioned properties the MAX-phases have become highly attractive materials for various technological and engineering applications. MAX phases have potential uses as high-temperature structural materials, porous exhaust gas filters for automobiles, heat exchangers, coatings for electrical contacts, heating elements, wear and corrosion protective surface coatings, electrodes, resistors, capacitors, biocompatible materials, rotating electrical contacts, cutting tools and nozzles, tools for die pressing and impact-resistant materials such as projectile proof armor [4–9]. Recently, MAX phases have become popular as neutron radiation resistant components for nuclear applications and 2D derivative (MXene) of MAX phases for using as energy storage materials and electrodes in micro-super capacitors, electrochemical capacitors, and batteries [10,11].

More recently, a report on the attractive electrochemical performance of Nb_2SnC in Li-ion electrolytes has been published, which has aroused widespread interest in the scientific community towards the Sn-containing MAX phases [12]. Two of the three MAX phases synthesized after this report are Sn-based MAX Phases. These two new members belong to 211 MAX family and they are V_2SnC and Sc_2SnC [13,14]. In the 211 MAX family, the other Sn-based members synthesized earlier were Lu_2SnC, Ti_2SnC, Nb_2SnC, Hf_2SnC and Zr_2SnC [15,16]. Now, there are a total of seven Sn-based compounds mentioned above in the 211 MAX family. Their structural, elastic, mechanical, lattice vibrational and thermal properties including defect processes have been investigated extensively [3,17–19]. Comprehensive study on optical properties of Sn-based 211 MAX phases is still absent. Kanoun et al. [20] investigated only the imaginary part of the interband frequency dependent dielectric function for four Sn-based 211 MAX phases namely, Ti_2SnC, Nb_2SnC, Hf_2SnC and Zr_2SnC. As the MAX phases are partially metallic compounds the inclusion of intraband transition is required to visualize the optical features accurately [21,22]. Detailed study of optical properties is only available for the Lu_2SnC and Nb_2SnC phases [1,23]. Therefore, a comprehensive and comparative study on the optical properties of the Sn-based 211 MAX phases is required. On the other hand, the attractive electrochemical performance of Nb_2SnC in Li-ion electrolytes has led to the usefulness of lithiation study of Sn-based 211 MAX phases. Also, insights into the nature of bonds can be gained by using the electron localization function (ELF), which has not yet been studied for the Sn-based 211 MAX phases. The amount of charge transfer among atoms can give a picture of the degree of ionicity in a particular MAX-phase compound. Considering these, we aim to investigate the optical response, lithiation and charge transfer in Sn-based 211 MAX phases with ELF in this study. Here we have employed first-principles density functional theory (DFT) within the CAmbridge Serial Total Energy Package (CASTEP) code and Vienna Ab initio Simulation Package (VASP), where appropriate. The rest of the paper has been organized as follows: Section 2 has been allocated for describing the computational methodology briefly. Section 3 has been used for presenting and discussing the results obtained in this study. Finally, Section 4 has been selected for summarizing the results with concluding remarks.

2. Computational methodology

Most of the DFT calculations in this study were carried out using the CASTEP code [24]. The electronic exchange-correlation energy was evaluated with the Perdew–Burke–Ernzerhof (PBE) functional within the generalized gradient approximation (GGA) [25]. Vanderbilt type ultrasoft pseudo-potential [26] was chosen to model the interactions between electrons and ion cores. A Γ-centered k-point mesh of 15 × 15 × 3 grid within the Monkhorst–Pack (MP) scheme [27] was employed to integrate over the first Brillouin zone in the reciprocal space of hexagonal unit cell of Sn-based 211 MAX phases. A cutoff energy of 700 eV was employed to expand the eigenfunctions of the valence and nearly valence electrons of atoms using a plane-wave basis. To optimize the geometry, the Broyden-Fletcher-Goldfarb-Shanno (BFGS) algorithm [28] was employed to minimize both the total energy and internal forces. To ensure the self-consistent convergence the difference in the total energy

was kept within 5×10^{-6} eV/atom, the maximum ionic Hellmann–Feynman force within 0.01 eV/Å, maximum ionic displacement within 5×10^{-4} Å, and maximum stress within 0.02 GPa. For lithiation calculation a supercell of 72 atoms was constructed for each phase and optimized with a plane-wave basis set cut-off energy of 450 eV and a k-point mesh of $3 \times 3 \times 2$-grid in MP scheme. Li interstitial was placed at all possible sites. After extensive searching for all possible sites, we found the minimum energy position of Li interstitial in each Sn-based MAX phase. Electron localization function (ELF) and Bader charge analysis were performed with the VASP code [29].

3. Results and discussions

3.1. Optical properties

The interaction of photons with the electrons in a crystalline solid can be described in terms of time dependent perturbations of the ground state electronic states. At present CASTEP provides two approaches to optical properties calculations; one is based on standard DFT Kohn-Sham orbitals and the other is based on time-dependent DFT (TD-DFT) theory, which is more precise but much more time-consuming. In this study, we have carried out the standard DFT optical calculations. In this approach the excited states are represented as unoccupied Kohn-Sham states. Transitions between occupied and unoccupied states are due to the electric field of the photon as the magnetic field effect is weaker by a factor of v/c. When these excitations are aggregated they are known as plasmons, which are utmost certainly observed by the passing of a fast electron through the system instead of a photon since transverse photons cannot excite longitudinal plasmons. When the transitions occur independently they are known as single particle excitations. The spectra due to these excitations are controlled by the joint density of states of the valence and conduction bands, weighted by appropriate matrix elements according to the selection rules concerning optical transitions.

Due to the hexagonal symmetry of the MAX phases, the polarization direction of the incident photon ⟨100⟩ and ⟨001⟩ are perpendicular to the direction of the corresponding electric field and parallel to the crystallographic c-axis, respectively. The MAX phases are partly metallic compounds and thus intraband transitions have a significant effect on the far infrared region i.e. the lower energy portion of the spectrum [30,31]. But, the goal of CASTEP is to demonstrate the optical properties of insulators and semiconductors and for this reason it does not consider intraband transitions by default. The intraband contribution to the optical properties can be confirmed by adding a semi-empirical Drude term to the optical conductivity in terms of the plasma frequency ω_P and damping parameter γ_D during optical calculations using CASTEP. The Drude damping parameter describes the broadening of the spectra due to effects of electron–electron scattering (including Auger processes), electron-phonon scattering, and electron-defect scattering. In general for metallic crystals, typical values of the plasma frequency, ω_p range from 2 to 10 eV and typical values of the Drude damping coefficient, γ_D ranges from 0.02 to 0.08 eV. For MAX and MAX-like compounds, the plasma frequency is chosen close to 3 eV and the Drude damping parameter is used as 0.05 eV [30–32]. In the present calculations, so we have used 3 eV and 0.05 eV as plasma frequency and Drude damping, respectively. However, 0.5 eV is used as Gaussian smearing in all optical calculations of metallic Sn-based 211 MAX phases.

The frequency-dependent complex dielectric function is a leading optical parameter, $\varepsilon(\omega) = \varepsilon_1(\omega) + i\varepsilon_2(\omega)$, consisting of real, $\varepsilon_1(\omega)$ and imaginary, $\varepsilon_2(\omega)$ parts. CASTEP uses the following equation to calculate the imaginary part of the dielectric constant:

$$\varepsilon_2(\omega) = \frac{2e^2\pi}{\Omega\varepsilon_0}\sum_{k,v,c}\left|\langle\psi_k^c|\mathbf{u}\cdot\mathbf{r}|\psi_k^v\rangle\right|^2\delta\left(E_k^c - E_k^v - E\right) \quad (1)$$

Here, ω is the phonon frequency, e is the charge of electron, Ω refers to the unit cell volume, $\mathbf{u}$ defines the unit vector along the polarization of the incident electric field and ψ_k^c and ψ_k^v denote the wave functions used for the conduction and valence band electrons at a particular k, respectively. The real and imaginary parts of $\varepsilon(\omega)$ are linked by a Kramers–Kronig relation. This relation is used to get the real part of the dielectric function:

$$\varepsilon_1(\omega) = 1 + \frac{2}{\pi}P\int_0^\infty \frac{\omega'\varepsilon_2(\omega')d\omega'}{(\omega'^2 - \omega^2)} \quad (2)$$

The other optical properties, such as the absorption coefficient, refractive index, extinction coefficient, energy loss-function, reflectivity and optical conductivity are calculated from $\varepsilon_1(\omega)$ and $\varepsilon_2(\omega)$ using the following equations:

$$\alpha(\omega) = \sqrt{2}\omega\left[\sqrt{\{\varepsilon_1(\omega)\}^2 + \{\varepsilon_2(\omega)\}^2} - \varepsilon_1(\omega)\right]^{1/2} \quad (3)$$

$$n(\omega) = \frac{1}{\sqrt{2}}\left[\sqrt{\{\varepsilon_1(\omega)\}^2 + \{\varepsilon_2(\omega)\}^2} + \varepsilon_1(\omega)\right]^{1/2} \quad (4)$$

$$k(\omega) = \frac{1}{\sqrt{2}}\left[\sqrt{\{\varepsilon_1(\omega)\}^2 + \{\varepsilon_2(\omega)\}^2} - \varepsilon_1(\omega)\right]^{1/2} \quad (5)$$

$$L(\omega) = \varepsilon_2(\omega) \Big/ \left[\{\varepsilon_1(\omega)\}^2 + \{\varepsilon_2(\omega)\}^2\right] \quad (6)$$

$$R(\omega) = \left|\frac{\sqrt{\varepsilon(\omega)} - 1}{\sqrt{\varepsilon(\omega)} + 1}\right|^2 \quad (7)$$

$$\sigma(\omega) = \frac{\omega\varepsilon_2}{4\pi} \quad (8)$$

Using equations (1)–(8) all the optical parameters of Sn-based 211 MAX phases are calculated for photon energy up to 20 eV. Following figures (1) and (2) represent the optical properties including dielectric function, refractive index, extinction coefficient, optical conductivity, reflectivity and loss function of Sn-based 211 MAX phases.

The real part of dielectric function, the most general property of a material, can characterize how a material responds to the incident electromagnetic wave of light. It is described for Sn-based 211 MAX phases in Fig. 1a for two polarizations. In both panels, the large negative value of $\varepsilon_1(\omega)$ at

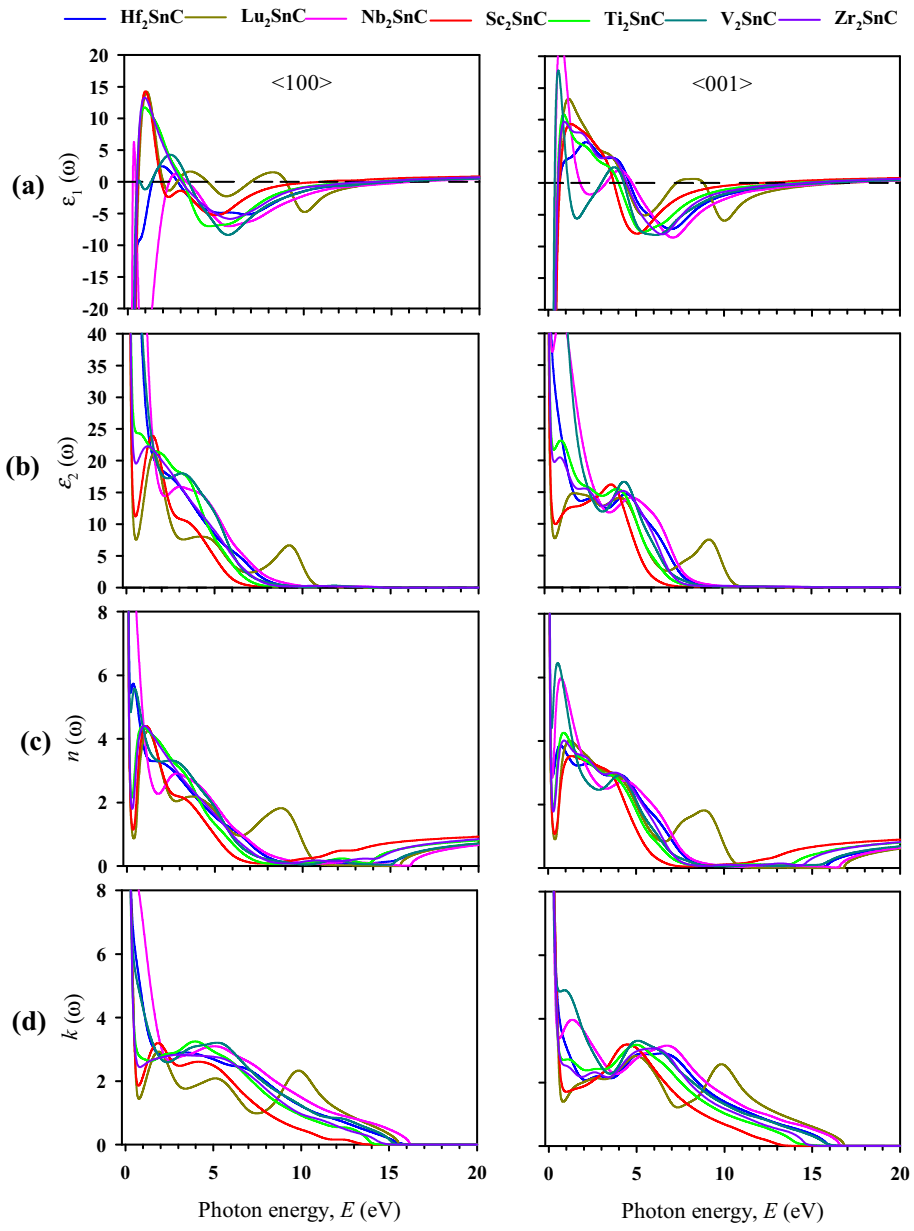

Fig. 1 – Optical parameters of M_2SnC MAX phases (a) real part of dielectric constant, (b) imaginary part of dielectric constant, (c) refractive index and (d) extinction coefficient. Left and right panels for the ⟨100⟩ and ⟨001⟩ polarizations, respectively.

the low energy part of the spectra shows the Drude-like behavior of Sn-based 211 MAX phases. The real part of dielectric constant (ε_1) approaches to zero from below, indicating the metallic nature of Sn-based 211 MAX phases. The non-zero value of $\varepsilon_1(0)$ is an indication of the large availability of free charge carriers in these metallic systems. For the polarization ⟨100⟩, all spectra reach the highest peak between 0.35 and 2.45 eV of incident photon energy. The spectrum for Nb_2SnC reaches its highest peak at the lowest energy of the photon while the spectrum for V_2SnC reaches at the highest peak at the highest energy of photon within the above mentioned range. Peak height is found to be large for Sc_2SnC and small for Hf_2SnC. The features for the polarization ⟨001⟩ are fairly different. For this polarization, the highest peaks spread between 0.58 and 2.15 eV of incident photon energy. The highest peak is observed for Nb_2SnC and the lowest peak is seen for Hf_2SnC. Up to 15 eV of photon energy, the anisotropic nature is significant.

The imaginary part of dielectric function $\varepsilon_2(\omega)$ is shown in Fig. 1b. It is linked to the dielectric loss and is always positive and characterizes the loss factor or energy absorbed by the material. The imaginary part of the dielectric function for both polarizations approaches zero from above. It is another indication of the metallic nature of the Sn-based 211 MAX phases. For two separate polarizations, the spectra of $\varepsilon_2(\omega)$ in the energy range of 0–11 eV exhibit a lesser anisotropic nature than

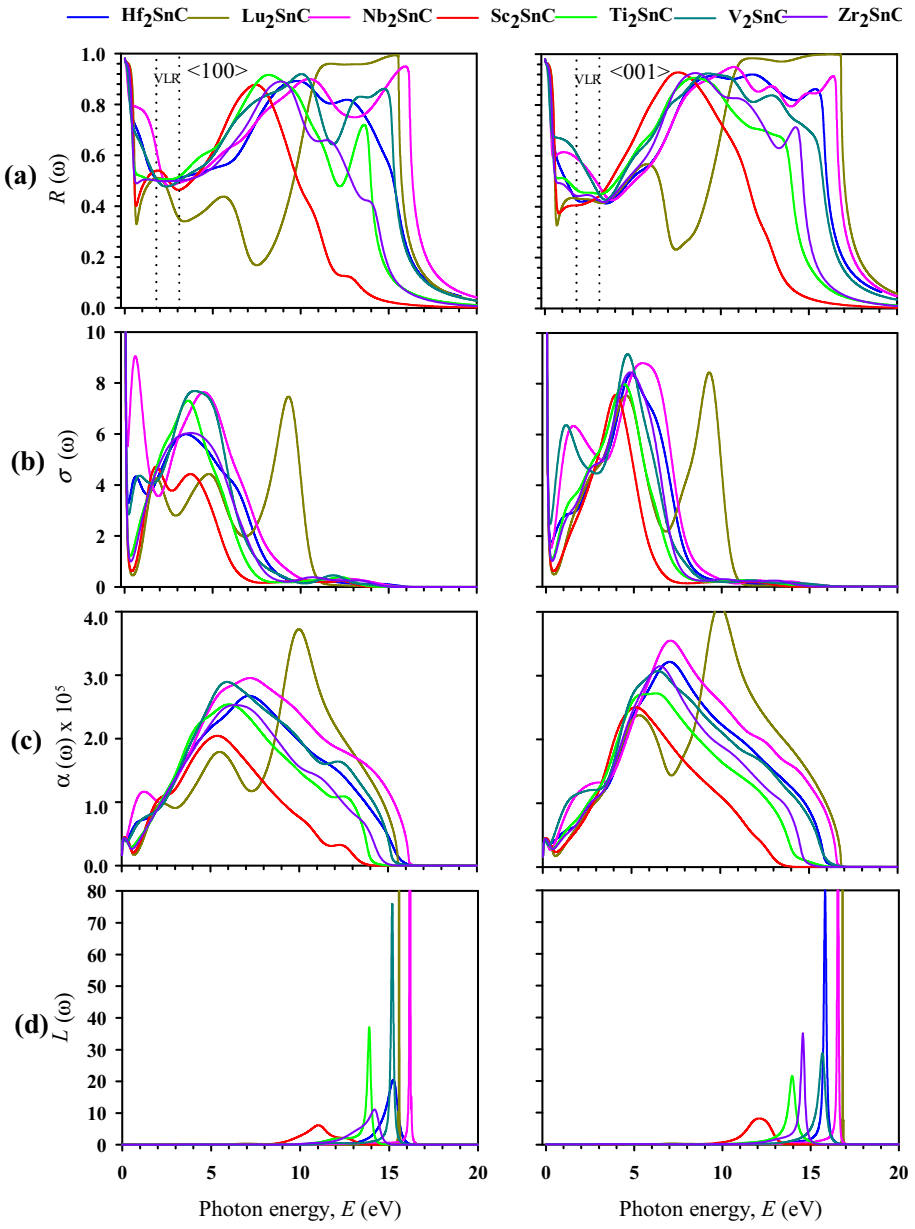

Fig. 2 – Optical parameters of M_2SnC MAX phases (a) reflectivity, (b) optical conductivity, (c) absorption coefficient and (d) energy loss function. Left and right panels for the ⟨100⟩ and ⟨001⟩ polarizations, respectively.

$\varepsilon_1(\omega)$ for the studied compounds. Lu_2SnC exhibits less anisotropic nature in $\varepsilon_2(\omega)$ among all Sn-based 211 MAX phases. The spectra for both polarizations in the high energy region are almost identical for all MAX phases under study.

The real part of the complex refractive index, also known simply as the refractive index, $n(\omega)$, shown in Fig. 1c, is another important optical property of materials. It indicates the phase velocity when the electromagnetic waves propagate through the material. A slightly anisotropic nature is observed in the $n(\omega)$ spectra for the Sn-based 211 MAX phases for the photon energy of both polarizations up to 5 eV. Above 5 eV of photon energy no significant anisotropy is observed for all members in the M_2SnC family.

The extinction coefficient $k(\omega)$, the imaginary part of the complex index of refraction, acts as an additional key optical parameter. It discloses the attenuation of electromagnetic radiation in a material and measures how strongly the material absorbs light at a particular wavelength per mass density or per molar concentration. $k(\omega)$ is associated with the conductive properties of the material. A metallic material has a large value of $k(\omega)$, while a semiconducting material has a small value of $k(\omega)$. Conversely, dielectric materials are basically nonconductors whose $k(\omega)$ value is zero. A large static value of $k(\omega)$ indicates the metallic conductivity of the Sn-based 211 MAX phases (refer to Fig. 1d). The spectra of $k(\omega)$ show considerable anisotropic nature for most of the Sn-

based 211 MAX phases for the photon energy of both polarizations up to 7 eV. Above this energy, the spectra show almost isotropic nature. It is consistent with a previous result for Nb_2SnC phases [23].

Optical reflectivity is an essential optical parameter that is linked to other optical functions and provides information regarding electronic structure of materials. Optical reflectivity calculated for Sn-based 211 MAX phases is shown in Fig. 2a. It is observed that the maximum (more than 98%) light is reflected for both the polarizations when photon is incident with low energy (frequency). High reflection of light at low frequencies indicates the high conductivity and low absorption power of the studied materials. Then there is a sudden decrease in reflectivity with an increase in photon energy. In the visible light region (VLR), the average reflectivity for both the polarizations is more than 40% for all the compounds studied here. This amount is sufficient for a compound to be a coating material for reducing solar heating. Considering the average for both the polarizations, optical reflectivity is highest for Nb_2SnC and lowest for Lu_2SnC in the VLR. The rank of possibility to be a coating material for M_2SnC MAX phases is: Nb_2SnC > V_2SnC > Ti_2SnC > Zr_2SnC > Hf_2SnC > Sc_2SnC > Lu_2SnC. In the higher energy side of the VLR the reflectivity increases rapidly up to ~9 eV for all phases except Lu_2SnC. At higher energies, Drude's approach begins to deviate, as the bound electrons of the metal atoms begin to respond to the light rather than simply the valence band electrons response. This leads to a decrease in reflectivity, which depends on the characteristics of the material. The reflectivity decreases rapidly at a characteristic frequency known as the plasma frequency of the material.

Optical conductivity is an important parameter that signifies the electrical conductivity in the presence of an alternating electric field. Optical conductivity is a good estimation of the photoconductivity of the materials [5]. Optical conductivity $\sigma(\omega)$ of M_2SnC MAX phases for both ⟨100⟩ and ⟨001⟩ polarizations is shown in Fig. 2b. A sharp peak in the optical conductivity spectrum near the zero frequency is an indication of the metallic nature of M_2SnC MAX phases. The spectra of both polarizations show significant variations in the range of photon energy from 0.5 to 5 eV, demonstrating the anisotropic nature in optical properties of Sn-based 211 MAX phases as found for Nb_2SnC in a previous study [23]. No compound in the M_2SnC family above 17 eV of photon energy is optically conductive.

The absorption coefficient $\alpha(\omega)$ determines how far light of a certain wavelength can penetrate a substance before it is absorbed. It also provides information on optimal solar energy conversion efficiency. Absorption coefficient $\alpha(\omega)$ of M_2SnC MAX phases for both ⟨100⟩ and ⟨001⟩ polarizations of light is shown in Fig. 2c. It is worth mentioning that like other metallic hexagonal systems the static absorption coefficient represents the universal non-zero value for the M_2SnC MAX phases studied here [21,22]. The spectral features are almost same for two different polarizations though the peak height is different. Indeed, light absorption between 0 and 8 eV is slightly higher for the polarization direction ⟨001⟩ for all compounds studied here except Lu_2SnC. Above 9 eV, the absorption of light is highest for Lu_2SnC for the ⟨001⟩ polarization. The absorption spectra of Nb_2SnC exhibit similar features reported in a previous study [23].

The energy loss function (in short, loss function) describes the amount of energy loss of fast electron moving in a material. Loss function $L(\omega)$ of M_2SnC MAX phases for both ⟨100⟩ and ⟨001⟩ polarizations is shown in Fig. 2d. Plasma oscillation causes a large peak in each spectrum in the energy range of 11–17 eV for both polarizations. The center of the highest peak indicates a distinctive frequency, known as the bulk plasma frequency, ω_p for each relevant material listed in Table S1. This characteristic frequency is found to be slightly larger for ⟨001⟩ polarization for all Sn-based 211 MAX phases. At this frequency the corresponding material changes from metallic to dielectric response and exhibits a rapid decrease in its reflectivity spectrum. Also, at this frequency the real part of the dielectric function becomes zero. The spectrum of energy loss shows no peak in the range of energy from 0 to 11 eV as a result of the large imaginary part of dielectric function $\varepsilon_2(\omega)$ [22]. For comparison we have found the ω_p of Nb_2SnC in literature [23]. The literature value of 15.4 V is slightly smaller than the obtained value of 16.2 eV. All optical properties are summarized in Table S1 for a convenient perception at a glance.

3.2. *Lithiation*

The formation energy in incorporation of a Li atom at the minimum energy interstitial position in the Sn-based 211 MAX phase, with ΔH for Li-incorporated systems, is defined by the following equation:

$$\Delta H = E(\text{with}x\text{Li}) - E(\text{without Li}) - xE(\text{Li}) \quad (9)$$

Where E(with xLi) and E(without Li) are the energies of the system with and without Li atoms. Here, we have used one Li atom as an interstitial, and as a result, $x = 1$. Also, E(Li) is the total energy of a single Li atom (here, it is calculated to be −192.024 eV). To calculate the energy of one Li atom, we constructed a bcc cell of metallic Li crystal, and we relaxed the geometry. We have calculated the energy of the cell in this way, and to find the energy of a Li atom we divided it by the number of Li atoms in the cell. Table 1 lists the formation

Table 1 – The formation energy of lithiated 211 Sn-based MAX phases.

Compounds	Formation energy (eV)	References
Hf_2SnC	2.10	This work
Lu_2SnC	0.36	This work
Nb_2SnC	2.26	This work
Ti_2SnC	2.83	This work
V_2SnC	2.80	This work
Zr_2SnC	1.76	This work
Sc_2SnC	0.94	This work
Ti_2C	2.26	[37]
Ti_3C_2	4.40	[38]
V_2C	0.96	[39]
Zr_2C	0.30	[33]
Sc_2C	0.31	[40]

energies of the lithiated Sn-based 211 MAX phases and some relevant MXenes. From Table 1, it is clear that the lithiation of the Sn-based 211MAX phases studied here is endothermic, reflecting instability. However, Lu_2SnC shows that Li formation energy is less than 0.5 eV, which makes it possible to incorporate Li into the MAX lattice, and it is even lower than those of MAX compounds considered in the previous works [33–35]. This is important because MXenes are usually considered better candidates for battery applications than MAX phases. Nevertheless, the present work has identified a compound Lu_2SnC that is potentially important for such applications. It should be emphasized that previous experimental works have only identified oxygen-doped Ti_3SiC_2 as having high Li-ion storage capacity, and therefore, as potentially important as an anode component for Li-ion batteries. In a previous study, it is found that Ti_3SiC_2 has high formation energy for lithiation [36]. This suggests that doping may further decrease the Li-intercalation formation energy of Lu_2SnC, making it a suitable candidate for battery applications.

It is instructive to note that MAX phases offer potential advantages over MXenes in certain respects, showing better material properties such as higher thermal-shock resistance, elastic stiffness, melting temperature and electrical and thermal conductivity. Moreover, they have less-complicated structures, as they do not require functional groups to be stable [33]. We have searched the literature on the formation energy of similar lithiated MXene structures and we summarize the available related theoretical data in Table 1. Clearly, similar MXenes exhibit lower formation energies compared to the MAX phases but still our calculated value for Lu_2SnC is one of the lowest reported formation energies for lithiation [33,37–40]. If we focus on the M_3C_2 family the only reported value of formation energy is equal to 4.40eV for Ti_3C_2. This value is higher than our theoretical results, so lithiation in the Sn-based 211 MAX phases can be deemed to be comparable with the MXene mentioned above.

3.3. *Charge transfer*

The amount of charge transfer among atoms can give a picture of the degree of ionicity in a particular MAX-phase compound. Charge transfer analysis was done using Mulliken [41] and Bader [42] methods. Mulliken method provides Mulliken charge as well as Hirshfeld charge while Bader method provides Bader charge. In contrast to the Mulliken method using local basis, the charge density of each atom was analyzed using only a spatial gradient of charge density in the Bader method. In Bader method, charge density is distributed in space and is divided into regions around the atoms. These regions, called Bader regions or volumes, are defined by surfaces that run through charge density minima. More accurately, along these surfaces, the gradient of the electron density has no component that is normal to the surface. The charges encased in the resulting Bader volumes are a good approximation for the actual charge state of an atom. The Bader charge and the Bader volumes are shown in Table 2 along with Mulliken and Hirshfeld charges.

The values in the table are the difference in the number of valence electrons and the results calculated with different methods for each Sn-based 211 MAX phases. The values obtained in the Bader method and the values obtained in the Mulliken method are generally not the same. The positive values in the table refer to the transfer of electrons from the atom and the negative values refer to the acceptance of electrons by the atom. According to Bader method, only M-atom transfers its charge into both Sn and C atoms. However, in the case of Mulliken charge for Hf_2SnC, Nb_2SnC and V_2SnC, the M-atoms as well as the Sn-atom take part in the charge transfer

Table 2 – Mulliken, Hirshfeld and Bader charges (in |e|) and Bader volume (in Å^3).

Compounds	Elements	Mulliken charge	Hirshfeld charge	Bader charge	Bader volume
Hf_2SnC	Hf	+0.28	+0.16	+1.378	14.538
	Sn	+0.31	+0.00	−0.837	27.143
	C	−0.86	−0.33	−1.918	13.630
Lu_2SnC	Lu	+0.45	+0.22	+1.027	20.290
	Sn	−0.46	−0.02	−0.504	29.440
	C	−0.43	−0.42	−1.549	13.460
Nb_2SnC	Nb	+0.31	+0.24	+0.683	16.669
	Sn	+0.07	−0.06	−0.245	22.272
	C	−0.68	−0.42	−1.120	09.007
Ti_2SnC	Ti	+0.42	+0.14	+0.799	13.169
	Sn	−0.11	+0.07	−0.398	23.469
	C	−0.74	−0.35	−1.200	10.434
Zr_2SnC	Zr	+0.43	+0.16	+0.881	18.367
	Sn	−0.07	+0.04	−0.434	25.486
	C	−0.78	−0.35	−1.328	10.699
Sc_2SnC	Sc	+0.53	+0.18	+0.952	15.523
	Sn	−0.21	+0.03	−0.548	28.853
	C	−0.85	−0.40	−1.356	13.140
V_2SnC	V	+0.32	+0.10	+0.661	11.973
	Sn	+0.01	+0.10	−0.238	21.475
	C	−0.64	−0.30	−1.085	09.189

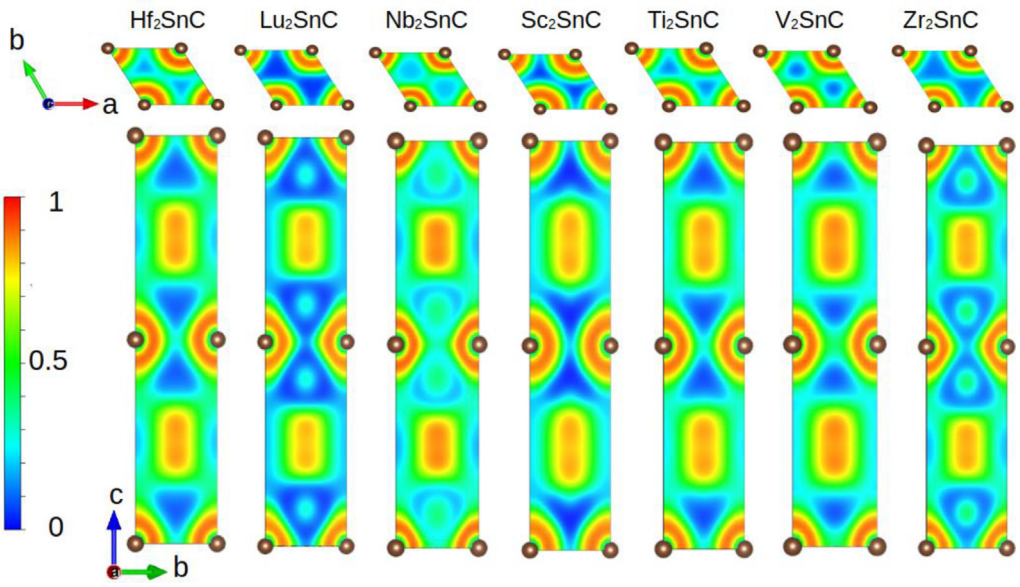

Fig. 3 – ELF maps for the [001] (top) and [100] (bottom) planes for the M_2SnC phases.

and in this case only the C atom takes up charge. Again, in the case of Hirshfeld charge for Hf_2SnC, Ti_2SnC, Zr_2SnC, Sc_2SnC and V_2SnC, the M-atoms as well as the Sn atom also take part in the charge transfer and in this case only the C atom takes up charge. The magnitude of the Bader charges is too large compared to the Mulliken and Hirshfeld charges. Although Mulliken charge analysis is widely used, Bader charge analysis is more acceptable than Mulliken and Hirshfeld charge analyses as it has a firm theoretical basis. According to Bader analysis, maximum charge transfer occurs in Hf_2SnC and minimum charge transfer occurs in V_2SnC.

3.4. *Electron localization function*

We have calculated the electron localization function (ELF), which was first introduced in 1990 by Becke and Edgecombe [43], as a measure of the probability of finding an electron in the vicinity of another electron with the same spin. Apparently, ELF is related to the same-spin electron pair probability density and calibrated with respect to a uniform electron gas so that it is dimensionless. It ranges between 0 and 1 and can give additional information on the location and the strength of the bonds. Regions that show high values of ELF (close to one) correspond to high electron localization where lower values, close to one-half, delocalized bonding is expected: values close to 0.5 correspond to perfect delocalization and a behavior similar to that of an electron gas, whereas values lower than 0.5 exist in areas between high concentrations of electron density [[44,45]].

In Fig. 3, the top and bottom panels show the ELF maps for the [001] and [100] planes, respectively. Additional representations have been shown in Fig. 4 for the [011] surfaces and the 3D maps with n = 1.0 and n = 0.5 can be found in Fig. S1 in the *Supplementary Section*. The regions around the carbon cores are characterized by high values of electron localization, in typical circular domains, as shown in Fig. 3 (bottom) for the carbon atoms and also in Fig. 4 for the metal ions, characteristic of the electron shells. The chemical bonds between metal ions and carbon (M-X) are expected to be strong localized bonds, which is supported by the ELF maps in both Figs. 3 and 4 with a combination of highly localized (red) regions surrounded by lower electron concentration (blue) regions, thus forming strong covalent bonds. The bonds between metal and Sn (yellow-green areas) are less localized and more spread out,

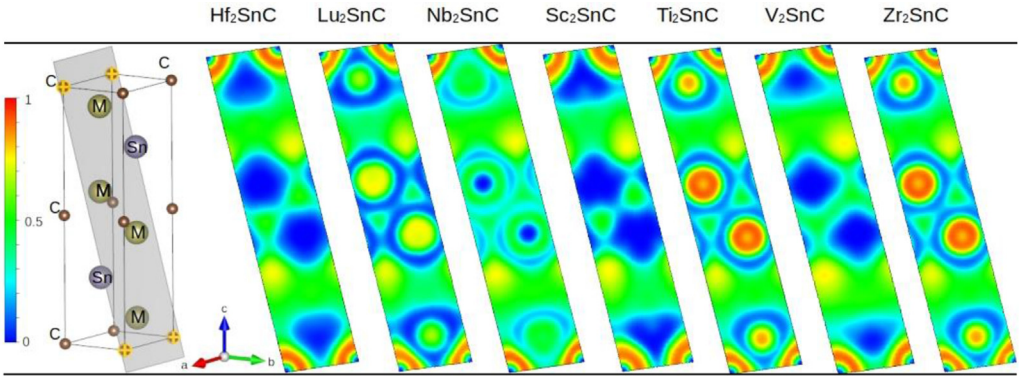

Fig. 4 – ELF maps along the [011] plane for the various M_2SnC phases.

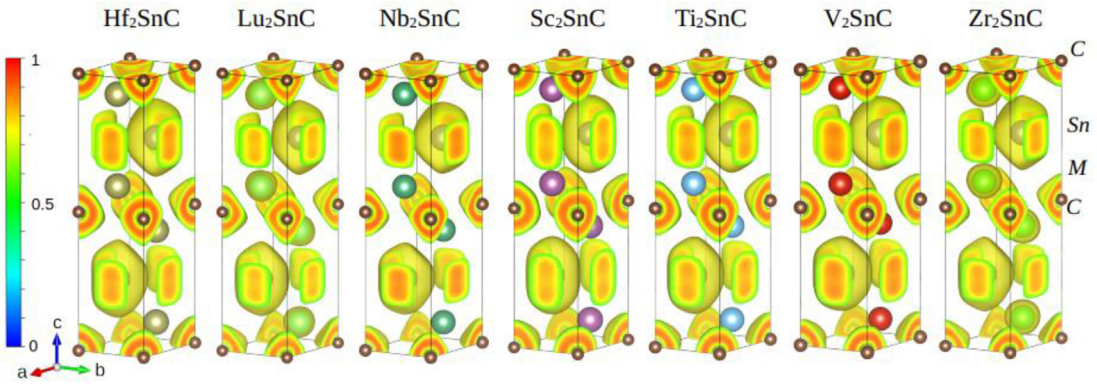

Fig. 5 – 3D ELF maps with n = 0.5 for the M_2SnC MAX phases.

possibly pointing to a weaker bond. Slight differences are shown between the various M_2SnC structures, which are related to the core radius and the number of electron shells. The ELF shows very low values for transition metal atoms, always lower than 0.5 as it is shown in Fig. 5.

4. Conclusion

In summary, DFT was employed to investigate the optical response, lithiation and charge transfer in Sn-based 211 M_2SnC MAX phases with ELF for the first time. Drude-like behavior was observed in the real part of dielectric function $\varepsilon_1(\omega)$ at the low energy region of the spectra for the compounds studied here. The large availability of free charge carriers in these metallic systems can be ensured by the non-zero value of $\varepsilon_1(0)$. Due to a large static value of extinction co-efficient $k(\omega)$ the Sn-based 211 MAX phases show the metallic conductivity. The spectrum of k (ω) shows significant anisotropic nature for most of the Sn-based 211 MAX phases up to 7 eV of photon energy for both polarizations. High reflection of light at the low frequencies is an indication of high conductivity and low absorption power of the studied materials. Since the average reflectivity exceeds 40% in the visible light region for both polarizations, all the compounds considered here have the potential to reduce solar heating as a coating material where Nb_2SnC is more likely. No compound in the M_2SnC family, above 17 eV of photon energy, shows optical conductivity. The static absorption coefficient represents the universal non-zero value for the hexagonal M_2SnC MAX phases studied here. The plasma frequency for polarization ⟨001⟩ is slightly larger and for all Sn-based 211 MAX phases the plasma frequency ranges from 11 to 17 eV. The inclusion of lithium (Li) in the Sn-based 211 MAX phases shows that the formation energy required for Li inclusion in the Lu_2SnC lattice is low, and therefore, it may be considered suitable for use as an anode in batteries. From the ELF maps, the chemical bond between the metal ion and the carbon (M– X) is considered to be the strong localized bonds. The bonds (M–Sn) between the metal atoms M and Sn appear to be less localized and more extended, indicating a weaker bond. Bader charges are much higher than the Mulliken and Hirshfeld charges in magnitude. According to Bader charge analysis, the highest charge transfer occurs in Hf_2SnC and the lowest charge transfer occurs in V_2SnC.

Credit authorship contribution statement

M.A.H. conceived the study. M.A.H., N.K., P.P.F and S.-R.G.C. carried out the calculations. M.A.H. and N.K. wrote the main manuscript text and prepared all figures. All authors reviewed the manuscript.

Data availability

Data will be provided on reasonable request.

Declaration of Competing Interest

The authors declare no competing interests.

Acknowledgements

The authors wish to acknowledge the High-Performance Computing (HPC) facility at Coventry University, Priory Street, Coventry CV1 5FB, UK and Institute of Nanoscience and Nanotechnology (INN), National Center for Scientific Research 'Demokritos', 15310 Agia Paraskevi, Athens, Greece for providing the computational facility to calculate the lithiation and ELF in M_2SnC MAX phase.

Appendix A. Supplementary data

Supplementary data to this article can be found online at https://doi.org/10.1016/j.jmrt.2022.03.083.

REFERENCES

[1] Hadi MA. Superconducting phases in a remarkable class of metallic ceramics. J Phys Chem Solid 2020;138:109275.
[2] Hadi MA. New ternary nanolaminated carbide Mo_2Ga_2C: a first-principles comparison with the MAX phase counterpart Mo_2GaC. Comput Mater Sci 2016;117:422–7.

[3] Hadi MA, Dahlqvist M, Christopoulos S-RG, Naqib SH, Chroneos A, Islam AKMA. Chemically stable new MAX phase V_2SnC: a damage and radiation tolerant TBC material. RSC Adv 2020;10:43783.
[4] Barsoum MW. The $M_{N+1}AX_N$ phases: a new class of solids; Thermodynamically stable nanolaminates. Prog Solid State Chem 2000;28:201–81.
[5] Mo Y, Rulis P, Ching WY. Electronic structure and optical conductivities of 20 MAX-phase compounds. Phys Rev B 2012;86:165122.
[6] Nappe JC, Grosseau P, Audubert F, Guilhot B, Beauvy M, Benabdesselam M, et al. Damages induced by heavy ions in titanium silicon carbide: effects of nuclear and electronic interactions at room temperature. J Nucl Mater 2009;385:304.
[7] Meng F, Chaffron L, Zhou Y. Synthesis of Ti_3SiC_2 by high energy ball milling and reactive sintering from Ti, Si, and C elements. J Nucl Mater 2009:386–8. 647.
[8] Wang J, Zhou Y. Recent progress in theoretical prediction, preparation, and characterization of layered ternary transition-metal carbides. Annu Rev Mater Res 2009;39:415.
[9] Eklund P, Beckers M, Jansson U, Hoegberg H, Hultman L. The $M_{n+1}AX_n$ phases: materials science and thin-film processing. Thin Solid Films 2010;518:1851.
[10] Tallman DJ, He L, Gan J, Caspi EN, Hoffman EN, Barsoum MW. Effects of neutron irradiation of Ti_3SiC_2 and Ti_3AlC_2 in the 121–1085°C temperature range. J NuclMater 2017;484:120–34.
[11] Shuck CE, Gogotsi Y, MXenes. A tunable family of 2D carbides and nitrides with diverse applications. Material Matters 2020;15:3–10.
[12] Zhao S, Dall'Agnese Y, Chu X, Zhao X, Gogotsi Y, Gao Y. Electrochemical interaction of Sn-containing MAX phase (Nb_2SnC) with Li-ions. ACS Energy Lett 2019;4:2452–7.
[13] Xu Q, Zhou Y, Zhang H, Jiang A, Tao Q, Lu J, et al. Theoretical prediction, synthesis, and crystal structure determination of new MAX phase compound V_2SnC. Journal of Advanced Ceramics 2020;9:481–92.
[14] Youbing L, Yanqing Q, Ke C, Lu C, Xiao Z, Haoming D, et al. Molten salt synthesis of nanolaminated Sc_2SnC MAX phase. J Inorg Mater 2021;36:773–8.
[15] Kuchida S, Muranaka T, Kawashima K, Inoue K, Yoshikawa M, Akimitsu J. Superconductivity in Lu_2SnC. Physica C 2013;494:77–9.
[16] Barsoum MW, Yaroschuk G, Tyagi S. Fabrication and characterization of M_2SnC (M = Ti, Zr, Hf and Nb). Scripta Mater 1997;37:1583–91.
[17] Hadi MA, Kelaidis N, Naqib SH, Chroneos A, Islam AKMA. Mechanical behaviors, lattice thermal conductivity and vibrational properties of a new MAX phase Lu_2SnC. J Phys Chem Solid 2019;129:162–71.
[18] Hadi MA, Kelaidis N, Naqib SH, Chroneos A, Islam AKMA. Electronic structures, bonding natures and defect processes in Sn-based 211 MAX phases. Comput Mater Sci 2019;168:203–12.
[19] Hadi MA, Christopoulos S-RG, Chroneos A, Naqib SH, Islam AKMA. DFT insights into the electronic structure, mechanical behaviour, lattice dynamics and defect processes in the first Sc-based MAX phase Sc_2SnC. Submitted to Scientific Reports; 2021.
[20] Kanoun MB, Goumri-Said S, Reshak AH. Theoretical study of mechanical, electronic, chemical bonding and optical properties of Ti_2SnC, Zr_2SnC, Hf_2SnC and Nb_2SnC. Comput Mater Sci 2009;47:491–500.
[21] Hadi MA, Roknuzzaman M, Nasir MT, Monira U, Naqib SH, Chroneos A, et al. Efects of Al substitution by Siin Ti_3AlC_2 nanolaminate. Scientifc Reports 2021;11:3410.
[22] Mitro SK, Hadi MA, Parvin F, Majumder R, Naqib SH, Islam AKMA. Effect of boron incorporation into the carbon-site in Nb_2SC MAX phase: insights from DFT. J Mater Res Technol 2021;11:1969–81.
[23] Nasir MT, Islam AKMA. MAX phases Nb_2AC (A = S, Sn): an ab initio study. Comput Mater Sci 2012;65:365–71.
[24] Clark SJ, Segall MD, Pickard CJ, Hasnip PJ, Probert MIJ, Refson K, et al. First principles methods using CASTEP. Z Kristallogr 2005;220:567.
[25] Perdew JP, Burke K, Ernzerhof M. Generalized gradient approximation made simple. Phys Rev Lett 1996;77:3865.
[26] Vanderbilt D. Soft self-consistent pseudopotentials in a generalized eigenvalue formalism. Phys Rev B 1990;41:7892.
[27] Monkhorst HJ, Pack JD. Special points for Brillouin-zone integrations. Phys Rev B 1976;13:5188.
[28] Fischer TH, Almlof J. General methods for geometry and wave function optimization. J Phys Chem 1992;96:9768.
[29] Kresse G, Furthmuller J. Efficient iterative schemes for ab initio total-energy calculations using a plane-wave basis set. Phys Rev B 1996;54:11169–86.
[30] He X, Bai Y, Chen Y, Zhu C, Li M, Barsoum MW. Phase stability, electronic structure, compressibility, elastic and optical properties of a newly discovered Ti_3SnC_2: a first-principle study. J Am Ceram Soc 2011;94:3907–14.
[31] Li S, Ahuja R, Barsoum MW, Jena P, Johansson B. Optical properties of Ti_3SiC_2 and Ti_4AlN_3. Appl Phys Lett 2008;92:221907.
[32] Li X, Cui H, Zhang R. First-principles study of the electronic and optical properties of a new metallic MoAlB. Sci Rep 2016;6:39790.
[33] Zhu J, Chroneos A, Eppinger J, Schwingenschlögl U. S-functionalized MXenes as electrode materials for Li-ion batteries. Appl. Mater. Today 2016;5:19–24.
[34] Zhu J, Chroneos A, Wang L, Rao F, Schwingenschloegl U. Stress-enhanced lithiation in MAX compounds for battery applications. Appl. Mater. Today 2017;9:192–5.
[35] Pang B, Mendes RG, Bachmatiuk A, Zhao L, Ta HQ, Gemming T, et al. Applications of 2D MXenes in energy conversion and storage systems. Chem Soc Rev 2019;48:72–133.
[36] Filippatos PP, Hadi MA, Christopoulos S-RG, Kordatos A, Kelaidis N, Fitzpatrick ME, et al. 312 MAX phases: elastic properties and lithiation. Materials 2019;12:4098.
[37] Wan Q, Shumming L, Liu J. First-principles study of Li-ion storage of functionalized Ti2C monolayer with vacancies. ACS Appl. Mater. Interfaces 2018;10(7):6369–77.
[38] Er D, Li J, Naguib M, Gogotsi Y, Shenoy VB. Ti_3C_2 MXene as a high capacity electrode material for metal (Li, Na, K., Ca) ion batteries. ACS Appl Mater Interfaces 2014;6:11173–9.
[39] Li Y-M, Guo Y-L, Jiao Z-Y. The effect of S-functionalized and vacancies on V_2C MXenes as anode materials for Na-ion and Li-ion batteries. Curr Appl Phys 2020;20(2):310–9.
[40] Lv X, Wei W, Sun Q, Yu L, Huang B, Dai Y. Sc_2C as a promising anode material with high mobility and capacity: a first-principles study. Chem Phys Chem 2017;18(12):1627–34.
[41] Mulliken RS. Electronic population analysis on LCAO–MO molecular wave functions. I. J Chem Phys 1955;23:1833.
[42] Henkelman G, Arnaldsson A, Jonsson H. A fast and robust algorithm for bader decomposition of charge density. Comput Mater Sci 2006;36:354–60.
[43] Becke AD, Edgecombe KE. J Chem Phys 1990;92:5397.
[44] Fuentealba P, Chamorro E, Santos JC. Understanding and using the electron localization function. [Chapter 5], Theoretical aspects of chemical reactivity. 2007.
[45] Burdett J, McCormick TA. Electron localization in molecules and solids: the meaning of ELF. J Phys Chem A 1998;102:6366–72.